Mathematical Blueprint of a Mitral Valve

Jiheum Park, PhD,[*,†] *Arnar Geirsson, MD, FACS,*[†] *and Pramod N. Bonde, MD, FACS*[*,†]

Mathematical modeling tries to simplify understanding and proposes a fundamental mechanism that governs the motion and function of a complex biological system such as a mitral valve (MV) motion which represents a dynamic interplay between papillary muscle (PM) position in the context of left ventricular (LV) shape dynamics. Current therapeutic strategies to intervene on the MV may not have exploited these relationships due to lack of understanding of the interactions. We present a MV 3D mathematical model characterized by LV shape dynamics to understand fundamental working principles of ventriculo-papillary-mitral complex. A complex 3D functional unit of MV apparatus was mathematically modeled based on a principle of dynamics. The model comprises of primary components including the annulus, anterior leaflet, posterior leaflet, chordae tendineae, anterior and posterior PM, and LV wall based on normal anatomical reference values from published series. Simulations based on Carpentier's classification of MV disease were created as well as based on LV shape dynamics and presented graphically. Autodesk Inventor (Autodesk Inc., San Rafael, CA) and Matlab (Mathworks, Natick, MA) were used for modeling and analysis. A stepwise analysis and mathematical models of the annulus, leaflets, chords, PMs, and LV were obtained by combining finite element analysis and computerized model creations. The model was then applied to Carpentier's functional classification. PM positions extrapolated based on different LV deformation in normal and mitral regurgitation (MR) model resulted in a different degree of MV leaflet coaptation with regurgitation (presented numerically and graphically). Abnormal MV coaptation was amended by manipulating PM positions independent with LV size or shape deformation, demonstrating that PM positioning maneuver may improve leaflet coaptation. LV dilation combined with increased interpapillary muscle distance turned out to intensify the level of leaflet prolapse, creating even greater regurgitation volume. Our mathematical model may provide a clue to complex interactions in play within a mitral, papillary, and LV complex. The model offers a possibility of manipulating various variables to obtain the desired outcome.

Semin Thoracic Surg 31:399–411 © 2019 Elsevier Inc. All rights reserved.

Keywords: Mitral valve, Mitral regurgitation, Papillary muscle, Left ventricle, 3D model, Mathematical model

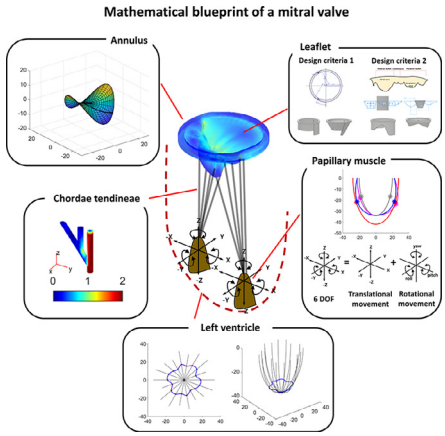

Mathematical characterization of mitral valve components and their synchronized interplay.

Central Message

Mitral valve is bound by a mathematical accuracy between components. The current study explores the mathematical blueprint of the mitral-papillary-ventricular complex.

Perspective Statement

Mitral valve (MV) is highly conserved among all vertebrates and is characterized by a complex dynamic interaction between the left ventricle and its leaflets. Understanding such a blueprint in mathematical sense has potential for diagnostic, therapeutic, and prognostic impact not only for MV disease but also for left ventricular dysfunction/failure.

Abbreviations: MV, mitral valve; LV, left ventricular; PM, papillary muscle; 2D, two-dimensional; 3D, three-dimensional; APM, anterior papillary muscle; PPM, posterior papillary muscle; e, eccentricity; CSI, Circular (Gibson) shape index; AR, aortic regurgitation; MR, mitral regurgitation; a/b, short to long-axis ratio; IPMD, interpapillary muscle distance; LVOT, left ventricular outflow tract; VTI, LVOT velocity time integral; LVdil, left ventricle dilation; PET, polyethylene terephthalate; STL, stereolithography

*The Mitral Laboratory, Yale School of Medicine, New Haven, Connecticut
†Section of Cardiac Surgery, Department of Surgery, Yale School of Medicine, New Haven, Connecticut

Disclosure: The authors have no conflicts of interest to disclose.

Address reprint requests to Pramod N. Bonde MD, FACS, Yale School of Medicine, 330 Cedar Street, New Haven, CT 06510. E-mail: pramod.bonde@yale.edu

1043-0679/$–see front matter

https://doi.org/10.1053/j.semtcvs.2019.01.008

INTRODUCTION

Characteristic of a vertebrate *heart* is its ability to pump blood to a vascular bed guarded by one-way valves and achieve adequate perfusion by maintaining a high-pressure gradient. A mathematical blueprint of one such valve, that is, mitral valve (MV) is highly conserved among all vertebrates[1–3] and is characterized by a complex dynamic interaction between a left ventricle (LV) and its leaflets. Understanding such a blueprint in a mathematical sense has the potential for diagnostic, therapeutic, and prognostic impact not only for MV disease but also for LV dysfunction/failure.

When viewed by conventional imaging techniques, MV apparatus is a functional unit having dynamic motions in 3 dimensions. Two papillary muscles (PM) situated at the distal part of LV are involved in spatial movement within LV shape deformation and productively communicate with MV leaflets via chordae tendineae. Currently, the optimal treatment option considered for MV disease is 2-dimensional (2D) manipulation of MV repair[4] leaflet plasties and annuloplasty ring to tighten dilated valve opening and improve leaflet coaptation. Tremendous improvement in terms of morbidity and mortality[5,6] in myxomatous valve disease has been achieved with surgical MV repair. However, poor long-term clinical outcomes with annular redilation[7] or high recurrence rate especially for severe ischemic mitral regurgitation[8] denote that we are perhaps overlooking the fundamental principle of 3-dimensional (3D) MV motion.

Controversy exists as to the optimal timing for MV repair, since current criteria of assessing LV function may not take into account subtleties of dysfunction. A robust technique to assess anatomical changes resulting in functional consequences with higher fidelity can potentially impact our criteria for interventions that are currently followed.

We have developed and report a detailed MV 3D mathematical model characterized by annular shape/size, leaflet-chordal interaction, LV shape dynamics, and effect of PM position on leaflet coaptation.

METHODS

We have presented mathematical design criteria for individual components of MV and how anatomical complexities can be added to it in a systematic way which allows quantitative analysis. Designs such as the annulus, leaflet, and chordae tendineae were created in Autodesk Inventor (Autodesk Inc., San Rafael, CA) and saved as stereolithography file format, which was then imported into Matlab (Mathworks, Natick, MA) for analysis and simulation. For finite element analysis, material properties of soft tissue (eg, Young's modulus of 60 kPa, Poisson's ratio of 0.4, and mass density of 1000 kg/m^3) have been applied to compute deformation and von Mises stress, a local failure criterion,[9] in response to pressure or forces applied.

A complete mathematical model of a complex 3D functional MV apparatus has been built based on the principle of dynamics[10] to carry out specific application studies (eg, spatial manipulation of PMs, mathematical interpretation of Carpentier's functional classification). The model comprises of primary components including the annulus, anterior leaflet, posterior leaflet, chordae tendineae, anterior papillary muscle (APM), posterior papillary muscle (PPM), and LV wall based on normal anatomical reference values from published series (Table 1).[11–16] The presented complete 3D mathematical model of MV represents its fundamental form and function, the mathematical blueprint of MV, where complexities can be further added on following our design criteria described for individual components as shown below. The detailed rationale and methodology for developing such 3D MV model are illustrated in Supplementary Material.

Table 1. Geometric Parameters and Material Properties Used for the Normal Model

	Model	Reference
Annulus diameter	35 mm	[11,12]22–40 mm
Anterior leaflet area	549 mm^2	[12]519 ± 108 mm^2
Posterior leaflet area	281 mm^2	[12]55 ± 71 mm^2
Anterior leaflet diameter	23.68 mm	[12]21.2 ± 3.0 mm
Posterior leaflet diameter	11.32 mm	[12]9.8 ± 2.0 mm
Leaflet thickness	4 mm	[13]3–5 mm
Interpapillary muscle distance	22 mm	[14]22 mm
PM tip to the annulus	23 mm	[11]23 mm
APM chordae tendineae length	15 mm	[12]18.8 ± 3.3 mm
PPM chordae tendineae length	18 mm	[12]19.3 ± 3.8 mm
Chordae tendineae stiffness	0.06 N/mm	[15]0.06 N/mm
Left ventricle dimension	34 mm	[16]32.4 ± 3.7 mm

Among the parameters shown, interpapillary muscle distance and left ventricle dimension are the only difference for the MR model from normal, where 30 Mm and 42 Mm have been used, respectively. Components of the mitral valve apparatus modeled include the anterior leaflet, posterior leaflet, annulus, papillary muscle, chordae tendineae, and left ventricle dimension. Superscript indicates references referred to.

Annulus

A mathematical expression of the mitral annular shape is that of a hyperbolic paraboloid that is elliptical when observed from the top view (which may not be entirely similar to the appearance of a usual horse saddle), although the side view may resemble more that of a horse saddle. The rim (as surgeons, we call it the annulus) of this hyperbolic paraboloid can then be thought of as a ring-shaped structure, which in mathematically correct term would be described as a curved toroid (biomimetic annuloplasty rings can be shaped as such, Fig. S1).

A conventional way of defining complex shape[17] of MV is discrete measurements of height, length, and width at specific locations rather than describing relationships among the measurements.[12,18] We have presented a mathematical equation of hyperbolic paraboloid which has a surface shape like a curved toroid can address the shape deformation of the annulus (Eq. 1, Fig. 1A).

$$z = \frac{(x-\alpha_L)^2}{a \cdot \alpha_V} - \frac{(y-\beta_L)^2}{b \cdot \beta_V} \quad (1)$$

where α_L and β_L are transformation parameters in lateral directions in xy plane, and α_V and β_V are transformation parameters in vertical directions in xz and yz planes, respectively. The other parameters of the denominator, a and b, are determined by

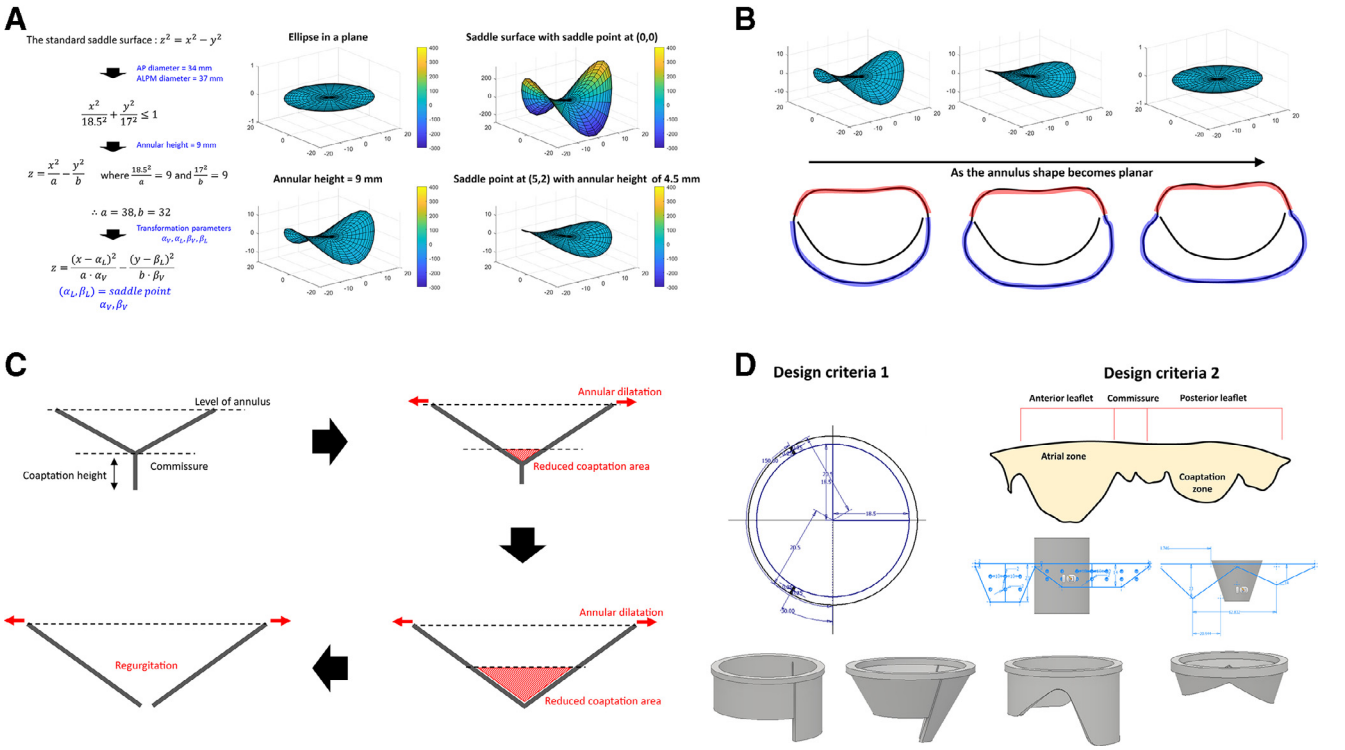

Figure 1. Mathematical creation of annulus and mitral leaflets. (A) Hyperbolic paraboloid equation to mathematically describe the complex toroidal shape of the annulus and its deformation. Transformation parameters shown on the block diagram determine the location or the degree of the curvature (Video 1). (B) As the annulus shape becomes a planar circle, the circumference of posterior dilates, while that of anterior remains. (C) Schematic illustration of decreasing coaptation area (Video 2). (D) Two exemplary mathematical design criteria for leaflets. One is by extruding cross-sectional area asymmetrically sectioned along either a cylinder or truncated cone to mimic longer circumference for the posterior and shorter for the anterior leaflet with different extruded lengths to mimic longer diameter for anterior and shorter for posterior. The other is by projecting stretched out mitral valve configuration onto either cylinder or truncated cone.

anteroposterior (AP), anterolateral-posteromedial diameter and annulus height. With α_L, $\beta_L = 0$ and α_V, $\beta_V = 1$, Eq 1 will represent undeformed hyperbolic paraboloid. Block diagram shown in Figure 1A illustrates the mathematical process of designing a complex toroidal shape of the annulus in 3D. The anticipated top and side views of the leaflets following this toroidal shape deformation are shown in Figure 1B and C, respectively.

Leaflets

Finite element analysis for soft tissue dynamics was used for analysis. Two design criteria can be considered for the leaflet design: (1) extrusion of cross-sectional area asymmetrically sectioned along either a cylinder or truncated cone and (2) projection of stretched out MV configuration onto either cylinder or truncated cone, which can be a more physiologically relevant way of design (Fig. 1D). In the first design criterion, circular, elliptical, or further complicated shape approximated through curve fitting (eg, spline, polynomial), for example, can define a cross-sectional area and asymmetrically bisected at defined anterior and posterior commissures so that posterior leaflet has longer circumference while anterior has the shorter one. Once the design for the cross-sectional area is completed, each bisected area can be extruded in different lengths so that posterior leaflet has shorter length while anterior has the longer one. Extrusion can be either along the cylinder or along the cone with defined lengths.

The second design criterion is inspired by in vivo leaflet specimen cut into a rectangular strip.[19] In the second design criterion, the configuration of the leaflet as a continuous piece of tissue is projected onto either hollow cylinder or hollow cone where the wall thickness is the leaflet thickness. Six different leaflet models were created using either design criterion 1 or 2. The second design criterion may provide an efficient way of reflecting morphologic differences exist between normal and diseased leaflets.[20]

The tested tissue was assumed to be linearly elastic and isotropic, with a typical Young's modulus of 60 kPa and Poisson's ratio of 0.4 as described in the previous study.[21] Assuming that blood pressure in LV would initiate leaflet coaptation, pressure on the outer surface of anterior and posterior leaflets has been given as a boundary condition to see different mechanical responses (eg, deformation) by different models (Fig. 2). Considering that the major stresses that act on the bending of each leaflet toward annulus would be the normal stresses, shear stress has been ignored.

Chordae Tendineae

Chordae tendineae is a complex network composed of primary, secondary, and tertiary chordae and it varies by patients, and

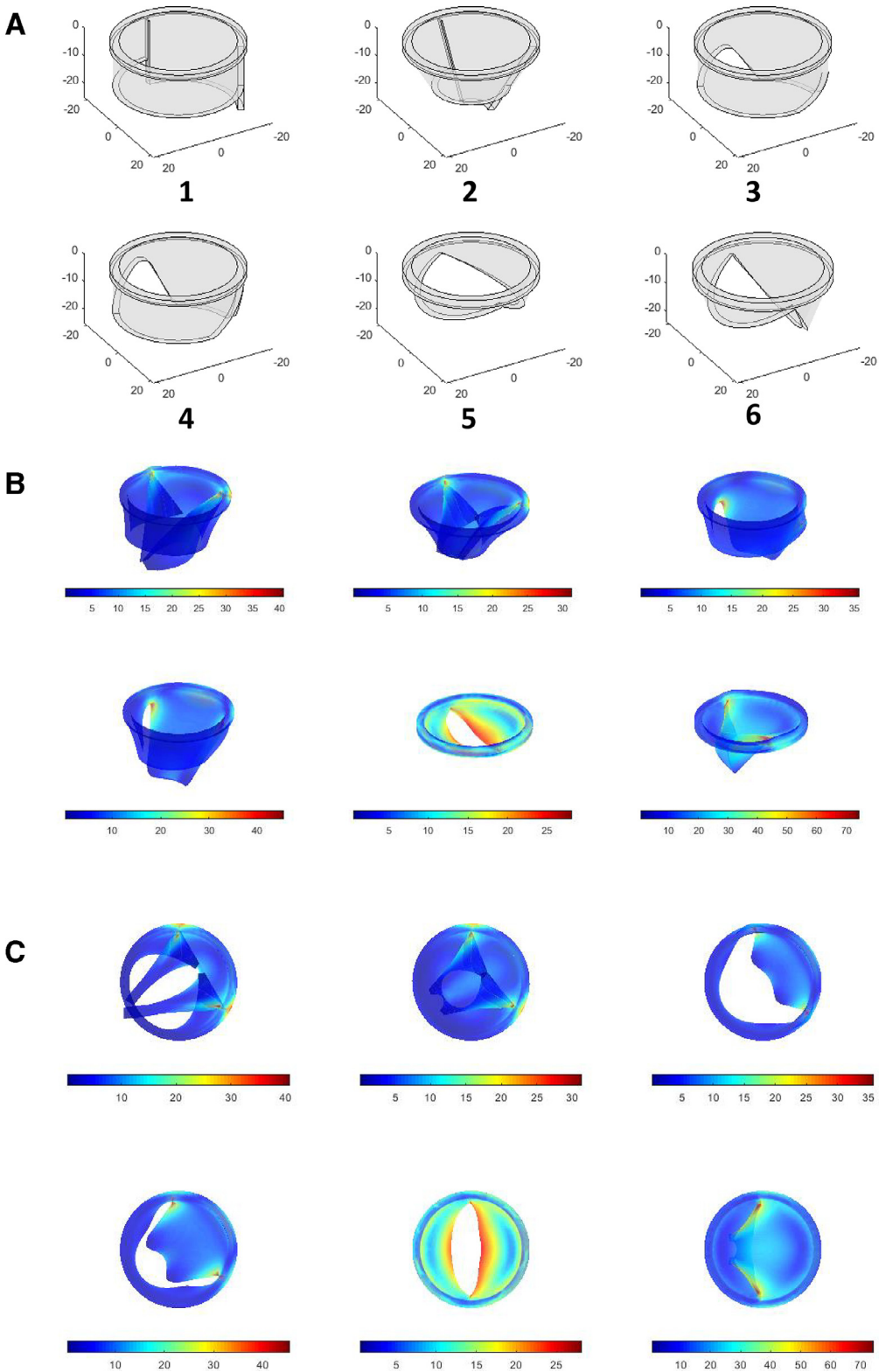

Figure 2. A plot of von Mises stress and deformation on 6 different leaflet designs in response to surface pressure applied to the leaflets based on finite element analysis. (A) Designs 1 and 2 follow design criterion 1 (Fig. 1D) within the cylindrical shape and truncated cone shape, respectively, and designs 3–6 follow design criterion 2 (Fig. 1D), within cylindrical shape for designs 3 and 4 and truncated cone shape for designs 5 and 6. Results of von Mises stress and deformation in side view (B) and top view (C) in response to the surface pressure of 0.1, 0.5, and 2 Pa for designs 1 and 2, designs 3 and 4, and designs 5 and 6, respectively.

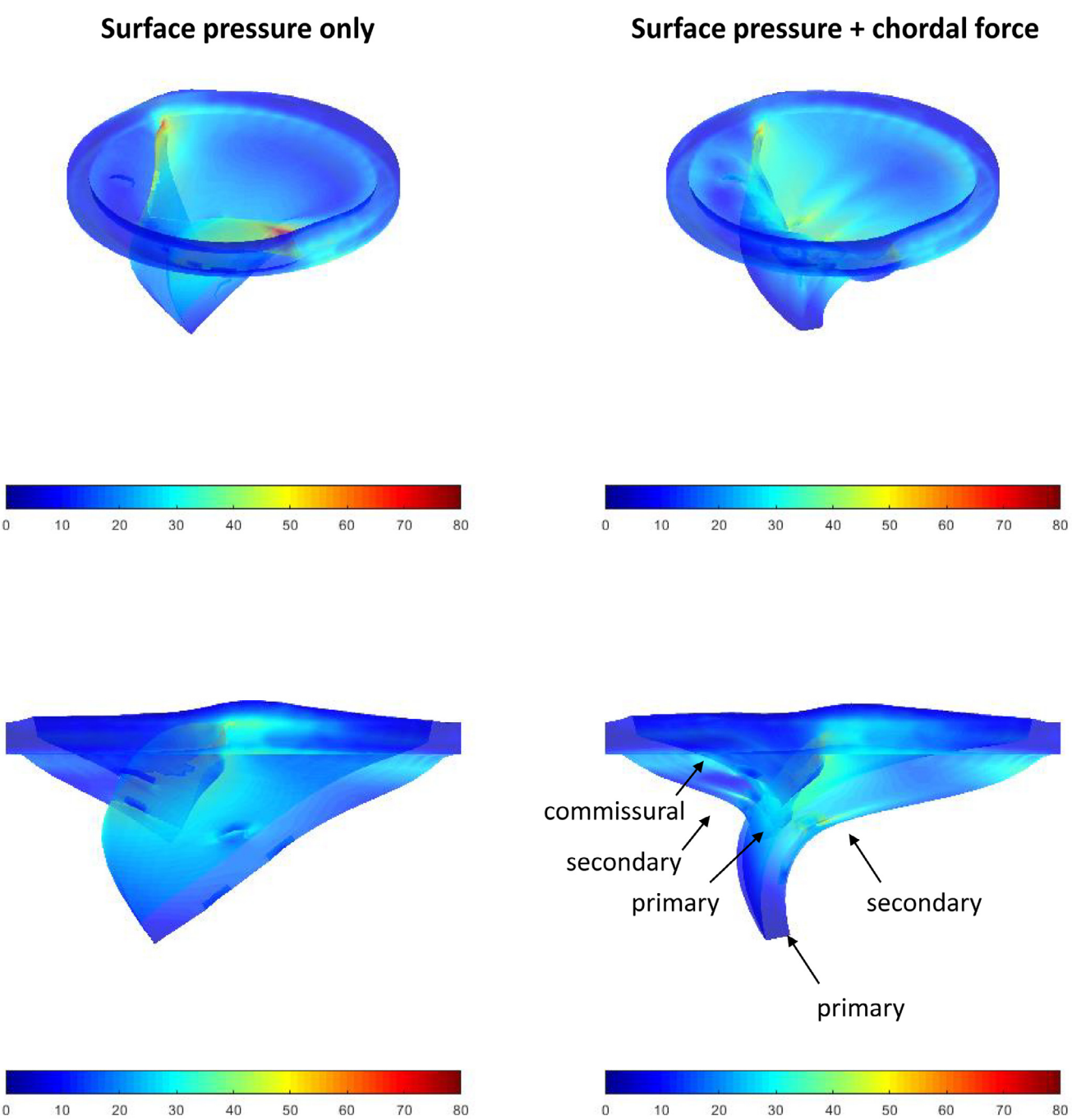

Figure 3. Finite element analysis on leaflet coaptation with and without chordal force. Primary, secondary, and commissural chords are incorporated. Proper chords attachment allows successful coaptation.

chordal force is an important supplement for successful leaflet coaptation (Fig. 3). However, most simulation studies on MV have focused more on contributions of blood volume and pressure measured in LV to successful leaflet coaptation rather than those of chordae tendineae. Chord dynamics has been relatively overlooked because it is rarely seen in echocardiography or MRI.[22,23]

Besides the matter of material properties of chordae tendineae whether viscoelastic or elastic, different angulation and branching points are also important variables[24] in manipulating leaflet coaptation as stress distribution can be significantly altered by its network (Fig. 4, Video 3).

For the chordal attachment on leaflets (Fig. 3), entire bottom-free edge surface of each leaflet was defined as primary chords attachment, and array of circles with a diameter of 2 mm was projected on outer surface of leaflets and extruded cut at a 0.5 mm depth in Autodesk Inventor design to define secondary and commissural chords attachment. Inward forces with defined directions, for example, toward the

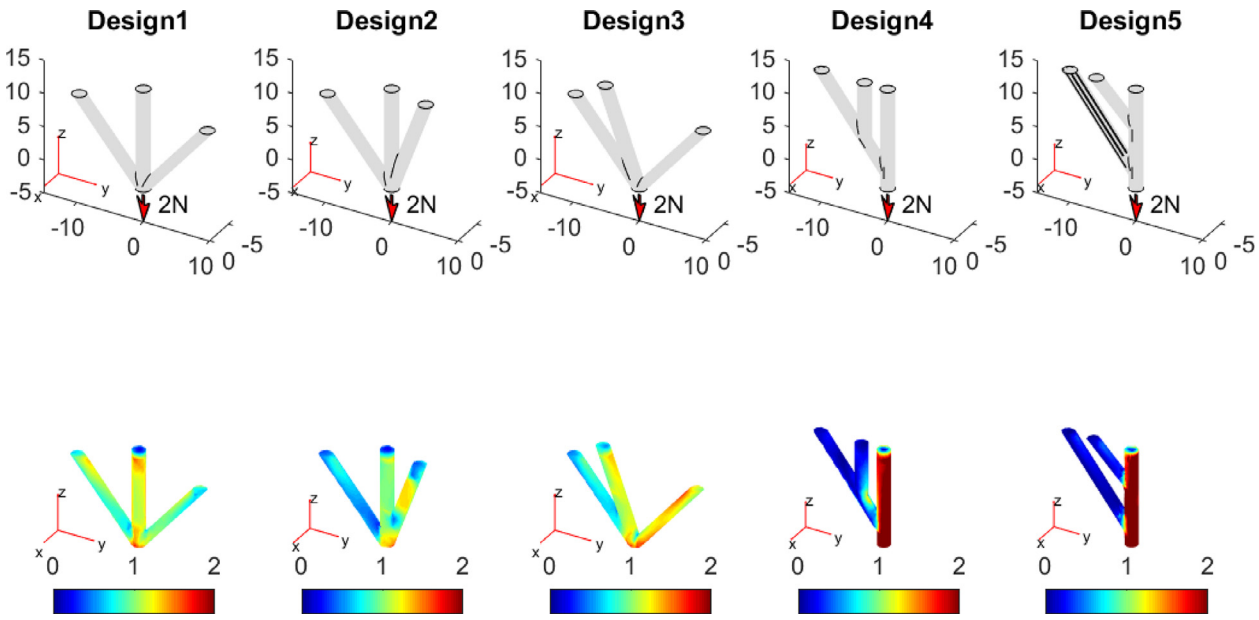

Figure 4. Variations in stress distribution by the different branching network of chordae tendineae. Stress distribution in 5 different chordae network designs when the bottom surface is pulled down in *z*-direction by the identical force of 2 N. Video 3 shows how the stress distribution varies by increasing the pulling force from 0 to 2 N.

center of annulus were applied to the surfaces of chordal attachment.

Papillary Muscles

Two PMs, APM and PPM, were attached to LV wall and interconnected with leaflets via chordae tendineae. Therefore, the motion of PM within LV dynamics plays a key role in the function of the mitral leaflet as its spatial motion results in force delivery to the leaflet via chordae tendineae. Spatial movement of PM can be mathematically interpreted as the motion in 6 degrees of freedom (6 DOF).

Left Ventricular Shape

Dynamic changes in LV shape during cardiac cycle alter by different disease states. Kass et al. evaluated 3 different methods (Fourier shape analysis, eccentricity [e], and Circular [Gibson] shape index [CSI]), mathematical techniques for analyzing curve, to characterize abnormalities of LV shape changes with aortic regurgitation (AR) and mitral regurgitation (MR),[25] addressing that neither eccentricity nor CSI adequately differentiates such abnormalities by its own. Accordingly, we attempted to characterize LV shape dynamics based on the combination of these 2 geometric indexes, which properly characterized normal, AR, and MR with corresponding short to long-axis ratio (a/b) given in the previous study[25] (Fig. S2). 6 DOF PM position was then extrapolated and redefined based on LV deformation as the intersection point between the LV outline and the line connecting LV center to PM base so that PM position places on LV outline and moves within LV shape deformation. The detailed method for extrapolating PM position changes according to the LV shape deformation can be found in Supplementary Material.

RESULTS

Modeling of Individual Component

Annulus

The elliptical boundary defined by AP and ALPM diameters determines that the size of the designed annulus and transformation parameters incorporated in the equation (Eq. 1) can mathematically define either location of the curvature or the degree of the curvature (eg, flattening the surface by reducing annulus height; Fig. 1A, Video 1). As the surface gets flattened and the annulus becomes a planar circle, the top view will display asymmetric dilation such that posterior circumference dilates while anterior circumference relatively remains (Fig. 1B), while the side view will display a reduction of coaptation area (Fig. 1C, Video 2).

Leaflets and Chordae Tendineae

Figure 2 shows the resultant plot of von Mises stress and deformation for each leaflet model in response to the blood pressure applied to the surface of leaflets. Since the pressure was applied normal to the surface curvature, leaflet deformation significantly varied by the leaflet conformation or its initial skew angle, allowing 2 leaflets come together but with a gap remained between, incomplete closure (Fig. 2B and C). To see the effect of chordal force distribution on successful coaptation, inward forces were given to the bottom surface of each leaflet, as primary chordal force distribution and forces in direction toward the center point of annulus were given to each circular spot designed at the surface of the leaflets as secondary and commissural chords attachment, which results in complete closure (Fig. 3).

6 DOF Motions of PMs and LV Shape (Deformation)

APM and PPM bases have been designed to have 6 DOF motion (Video 4) within LV wall dynamics and their tips as well in the same way to mimic their own muscle contraction and relaxation (Video 5).

For the LV wall dynamics, we have presented a new way of characterizing abnormalities of LV shape changes with AR and MR distinct from those with normal (Fig. S2). Mathematical description of ventricular dilation can be further sophisticated by incorporating egg shape instead of an ellipse, and using the same a/b that characterizes different disease states, to address asymmetric dilation. Figure 5A and Video 6 show the mathematical description of symmetric or asymmetric LV dilation in 2 dimensions within PM position changes based on the LV shape deformation.

This 2D way of describing LV shape deformation can essentially be turned into 3D. A half rotation (180°) of 2D planes where the different elliptical shape is defined at each angle can address complex 3D morphologic features of LV shape which depends upon disease etiology (Fig. 5B, Video 7).

Application Study With the Complete 3D Model of Mitral Valve

Spatial Manipulation of Papillary Muscles

Normal (Video S1) and 3 different MR models, MR model I (Video S2), II (Video S3), and III (Video S4) were presented. By showing that reduced leaflet coaptation can be amended by rearranging PM positions in the MR model while maintaining other conditions the same as those in MR models such as LV size, LV shape deformation, or annulo-PM distance, we were able to highlight that spatial manipulation of PM can improve leaflet coaptation (MR-fixed model, Video S5).

Carpentier's Functional Classification

Additionally, we report a mathematical interpretation of Carpentier's functional classification based on our simulation model, which can address annular dilatation, PM rupture, leaflet calcification, PM displacement, chordae tethering, and LV dilation on leaflet coaptation. We considered representative features for each classification (Table 2). Simulation results for

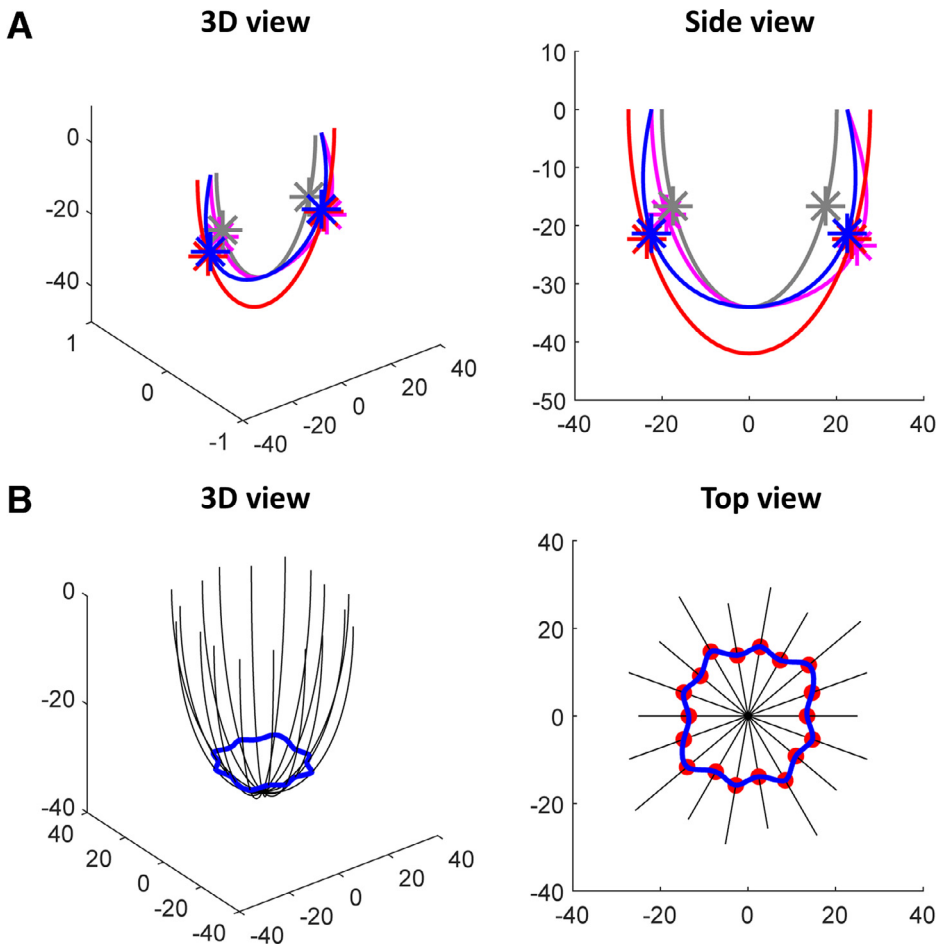

Figure 5. Mathematical description of left ventricular shape (LV) deformation in 2D and 3D. (A) Mathematical description of symmetric or asymmetric LV shape deformation in 2D and papillary muscle position changes according to this LV shape deformation (Video 6). (B) Mathematical description of LV shape deformation in 3D. Complex 3D shape LV during its deformation can be mathematically described by spanning multiple of different 2D elliptical shapes shown in (A) over 180° (Video 7).

Table 2. Mathematical Interpretation of Carpentier's Functional Classification

Dysfunction	Clinical Lesions	Mathematical Modeling
Type I	Annular dilatation	Increased annular diameter
Type II	Elongation/rupture chordae	Selected chordae stiffness = 0
	Elongation/rupture of papillary muscle	Entire chordae from either anterolateral or posteromedial papillary muscle stiffness = 0
Type IIIa	Leaflet thickening/retraction	Increased leaflet mass
	Leaflet calcification	
	Chordal thickening/retraction/fusion	
	Commissural fusion	
Type IIIb	Papillary muscle displacement	Increased interpapillary muscle distance without dilated ventricle
	Chordae tethering	Downward displacement of papillary muscle
	Left ventricular dilation/aneurysm	Dilated ventricle

type I (Video S6), II (Videos S7 and S8), IIIa (Video S9), and IIIb (Videos S10 and S11) disease are presented. Detailed methods (Fig. S3) and results (Figs. S4 and S5) for our simplified 3D mathematical model of MV are described in Supplementary Material.

DISCUSSION

In this study, we have proposed a simplified mathematical model that codifies complex biological interactions within annulus, leaflets, chords, PMs, and LV in mathematical terms. The mathematical basis for the shape of the mitral annulus (a curved torus) and how to derive it was proposed, leaflets were analyzed using finite element analysis to demonstrate interactions between LV pressure and chordal attachments in coaptation. Chordal stress and its interactions were analyzed together with the performance of such mathematical systems within the Carpentier's functional classification of MV pathology. We further show the role of 6 DOF PMs manipulating leaflet motion and tailoring MV prolapse by PM rearrangement. All influential factors on leaflet motion such as annular diameter, ventricular shape, PM positions, and chordal rupture or elongation work in unison to alter the forces acting on the leaflets and leading to moving objects in 3 dimensions. Keeping this perspective from the current study, the most common treatment option of MV annuloplasty which is based on 2D regulation of the force acting on the leaflet may have limitations if the pathology in question is other than annular dilatation or excessive leaflet prolapse.

MV anatomy and mechanics remain highly conserved among animal phyla when one considers the flow of blood from atrium to the systemic ventricle in comparative anatomical studies.[1–3] Understanding this mathematical blueprint is crucial when one wants to elucidate the various relationships between the complex structures such as MV. This is more so important when one wants to test the influence of manipulating different anatomical structures to obtain a clinically "competent" valve.

Guidelines and recommendations about the timing of intervention on MV are based primarily on historical outcomes with surgical therapy and attendant mortality. Subsequent recommendations were based on improved surgical techniques nearing zero mortality in expert centers when the likelihood of repair was considered very high. These thresholds for intervention are based on LV dimensions and ventricular function (as measured by ejection fraction). However, MR, except when it presents as acute presentation (chordal rupture, PM rupture as a result of myocardial infarction), is a chronic disease process with usually an ability to follow patients longitudinally. As different therapeutic interventions are being proposed (such as Transcatheter Mitral Valve Replacement (TMVR), new chordal placement, leaflet approximation techniques, annuloplasty cinching techniques, ventricular shape modifiers, and PM approximations), some with the endovascular approach with very low morbidity, we may have to re-examine our thresholds for intervention on MV. For example, can we intervene early, so left atrial/ventricular dilatation and dysfunction can be prevented and thus reducing morbidity with MR-associated adverse events.

Such intervention will need to be able to address and measure MV dysfunction in much more depth beyond current criteria for regurgitant volume, LV dilatation, and ejection fraction. For example, with improved repair techniques, one would argue for earlier intervention before LV dilatation takes place. The current mathematical blueprint is designed to address some of these questions. Morphology and properties of leaflet vary by patients, addressing the importance of customized therapy for MV disease. Our leaflet model was directly designed through 3D computer-aided design software and imported as stereolithography file with given information about mass, shape, and geometry based on the design created and material properties chosen. Instead, importing 3D-scanned MRI and Echocardiography (ECHO) images can be imported with patient-specific biomechanical properties, which can easily create a patient-specific mitral-papillary-ventricular model. Such individualized model can be used to study patients temporally and across interventions.

Limitations

The source of force variations in the complete 3D mathematical model of MV affecting leaflet motion by different PM orientations is chordae tendineae, which was modeled as massless springs in our mathematical model with 10 chordae tendineae attached to each leaflet, 5 from APM and the other 5 from PPM, in equally spaced manner at free margin of the leaflet,

which denotes primary chordae only. Precise mimicry of in vivo chordae tendineae, for example, with viscoelastic properties[26] can potentially improve the current mathematical model in terms of prediction accuracy. Particularly, incorporation of secondary chordae in the model may provide additional insights, as primary and secondary chordae are known to have different functions such that primary chordae is more involved in MV competence while secondary chordae is more involved in LV geometry with greater tension.[27,28]

Clinical Relevance

MV apparatus is generally divided into multiple components and interpreted individually. Considering close interplay among the components, MV can be described in a single functional unit. This has direct implications when one considers a serial examination of a degenerative MV apparatus across a timeline. For example, with an introduction of electronic storage of imaging data, an algorithm based on the mathematical model can provide important information in actual structural and visual format with data collated from series of imaging studies over time. Currently, as surgeons, we employ mostly our ability to detect changes in the anatomy over the years relying on experience and wait till more hemodynamically significant issues have brought the patient for the consultation. Parameters can be studied across populations samples (some of the data already exist in the imaging libraries) to set triggers for intervention or more close monitoring.

It is easily possible to superimpose patient imaging data on a 3D structural unit proposed in the present manuscript. Surgeons will be able to virtually compare what type of surgical intervention will result in the reduction of regurgitant volume or exacerbate it or likely lead to failure of repair. A failure rate/likelihood ratio can be computed by utilizing the mathematical blueprint in this investigation to guide surgeons while discussing with patients the various therapeutic choices. This can also aid multidisciplinary *heart* teams while making a selection for surgical vs nonsurgical or catheter-based approach and combine this to the patient's other risk factors.

The utility of this tool can be further realized by its value as a teaching aid prior, during, and after surgery. Furthermore, causes of failure of interventions on MV in ischemic or dilated cardiomyopathy patients can be predicted based on the LV dynamics, alerting surgeons for exploring replacement strategies instead of leaflet/annulus repair strategies alone.

One example of direct clinical impact may be the evidence that we have shown for improving leaflet coaptation by PM rearrangement in 3 dimensions. Proper PM positioning to reduce MR may differ by patients, which may partially validate current treatment option PM approximation in the form of PM sling.

Prior studies have attempted simulation with reconstructed mitral leaflet morphology by importing 3D-scanned MRI or ECHO images from patients, which is compatible with our mathematical model, with added ability to interpret morphologic changes or differences from one another in a quantitative way. The interpretation will not be limited to measuring average height, length, and width at specific locations but will also include relationships among the measurements. We have presented how the deformation of the annulus and leaflet shape can be mathematically described. Our technique may lead to the different way of analyzing malfunction of MV with quantitative measurements by finding a source of transformation and thereby finding exact locations where force needs to be applied to improve leaflet coaptation, thereby providing patient-specific repair solution.

CONCLUSION

We have built a mathematical blueprint of a human mitral-papillary-ventricular complex which has a potential for understanding various variables that can influence MV function and its effect on LV geometry. As an example, our mathematical model has shown the potential of manipulating subvalvular elements to influence leaflet coaptation. This is corroborated by normal, MR, and MR-fixed model with successful leaflet coaptation, leaflet prolapse, and leaflet prolapse corrections, respectively, under different PM orientations extrapolated according to LV shape deformation. Different PM orientations were able to show anterior prolapse with normal posterior motion and vice versa, demonstrating independent control of anterior and posterior leaflet. Likewise, simulation of Carpentier's functional classification has shown that how each lesion can be mathematically interpreted and applied to the model.

SUPPLEMENTARY MATERIAL

The following is the supplementary data to this article:

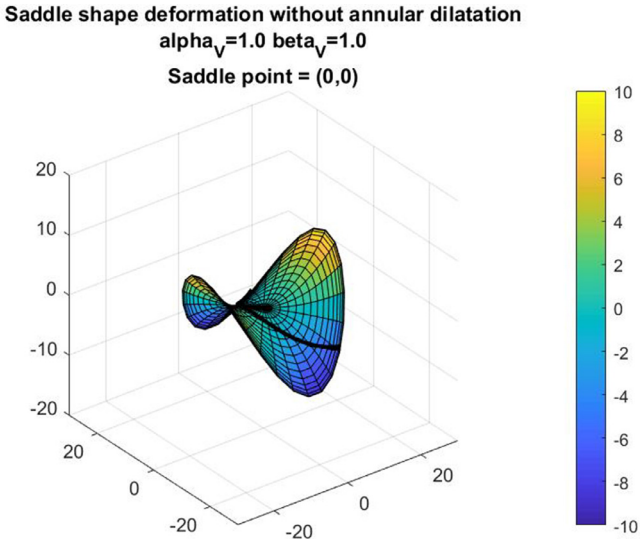

Video 1. Mathematical description of the saddle shape of an annulus and its deformation. The mathematical equation of hyperbolic paraboloid which has a surface shape like a saddle can address the shape deformation of the annulus. The elliptical boundary defined by anteroposterior (AP) and anterolateral-posteromedial ALPM diameters determine the size of the designed annulus and transformation parameters incorporated in the equation can mathematically define either location of the curvature or the degree of the curvature (eg, flattening the surface by reducing annulus height).

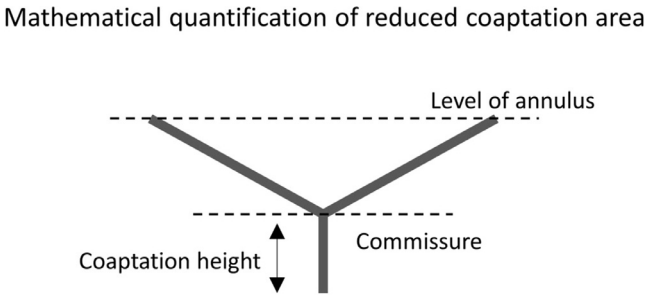

Video 2. Animated depiction of reduction in coaptation area. As annulus conformation gets flattened and becomes a planar circle, the top view will display asymmetric dilation such that posterior circumference dilates while anterior circumference relatively remains, while the side view will display a reduction of coaptation area.

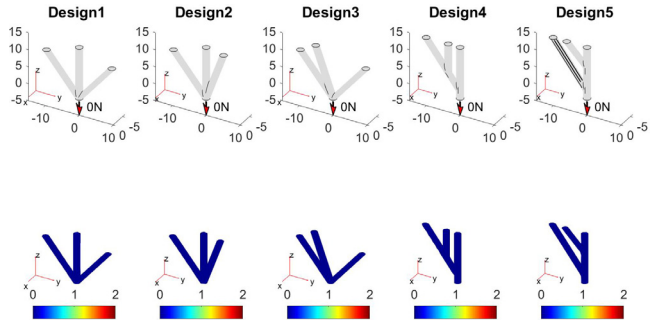

Video 3. Variations in stress distribution by a different branching network of chordae tendineae. Different angulation and branching points are important variables in manipulating leaflet coaptation as stress distribution can be significantly altered by its network.

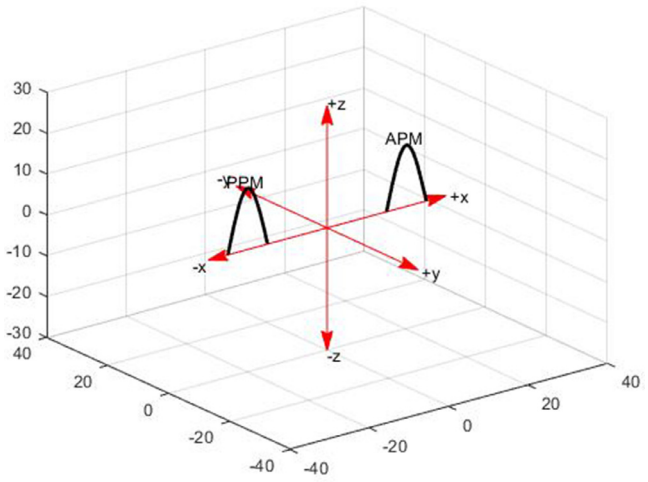

Video 4. Papillary muscles 6 degrees of freedom motions. APM and PPM bases are designed to have translational as well as rotational movement in respect to 3 axes (X, Y, and Z) to mimic the evidence that PM positions relative to the leaflets represented by LV deformation and annulus movement are in 3D motion.

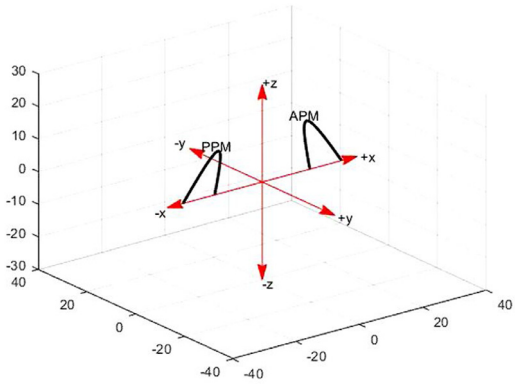

Video 5. Synchronous contraction of papillary muscles. APM and PPM tips can be designed to have 6 DOF motion to mimic their own muscle contraction and relaxation. In our current simulation, default motion of the tip was set to tilt inward 2.5° at each simulation run for both PMs and total 10° by the end of the simulation.

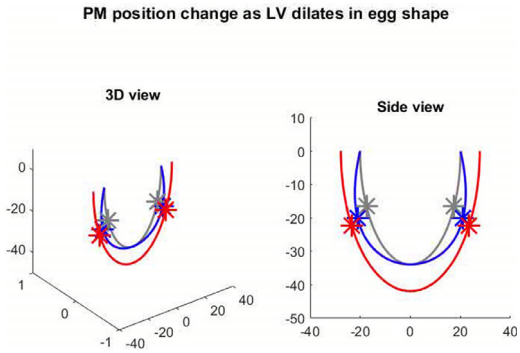

Video 6. Papillary muscle position extrapolation by LV shape deformation. Mathematical description of symmetric and asymmetric left ventricular (LV) shape deformation. Papillary muscle position changes according to the LV shape deformation.

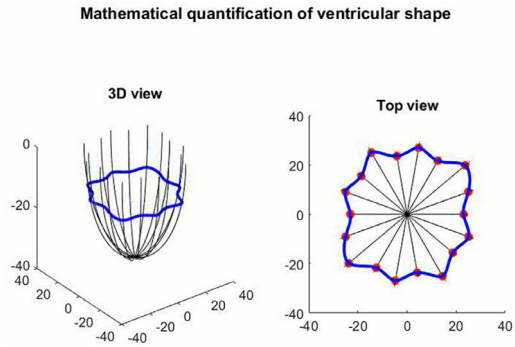

Video 7. Mathematical description of ventricular shape in 3D. Different elliptical shape defined by 2 geometric parameters (e, eccentricity and CSI, Circular [Gibson] shape index) can describe the shape of the left ventricle at multiple 2D section views arrayed in different angles in respect to z-axis. Thus, the 180° spanning of these elliptical shape outlines about z-axis can address complex 3D shape of the left ventricle and its shape deformation quantitatively.

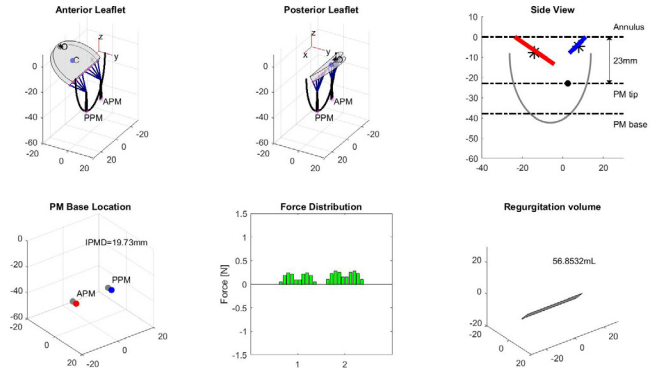

Video 8. Simulation runs for normal model. Anterior and posterior leaflets shown in the first and the second panels in the top row are initially at a downward position at end diastole and moves toward annulus as left ventricle contracts during systole. 2D side view of the mitral valve model in the third panel clearly shows changes in vertical positions of each component relative to each other, such as changes in the annulo-PM distance during simulation runs. The fourth panel, the first panel in the bottom row shows changes in interpapillary muscle distance where both APM and PPM positions start at ΔXYZ = (0, 2.5, 0) for the normal model. The fifth row shows variations in force distribution exerted on leaflets as the length of chordae tendinea changes. The sixth row shows changes in the opening area created between the anterior and posterior leaflets which are used to estimate regurgitation volume. Successful coaptation can be seen in normal model.

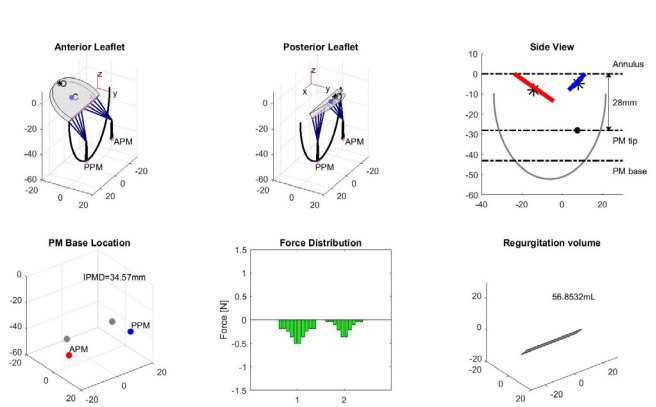

Video 9. Simulation runs for MR model I. While the normal model was built based on normal ventricular dynamics with ventricular size of 34 mm, interpapillary muscle distance of 22 mm, and consistent annulo-PM distance, MR model was built based on MR ventricular dynamics with increased ventricular size of 42 mm, increased interpapillary muscle distance of 30 mm, and decreasing annulo-PM distance. PM position rearrangement with ΔXYZ = (−5, 7.5, −5) for APM and ΔXYZ = (5, 7.5, −5) for PPM resulted in anterior leaflet prolapse with posterior leaflet tethering creating regurgitation volume of 37.08 mL.

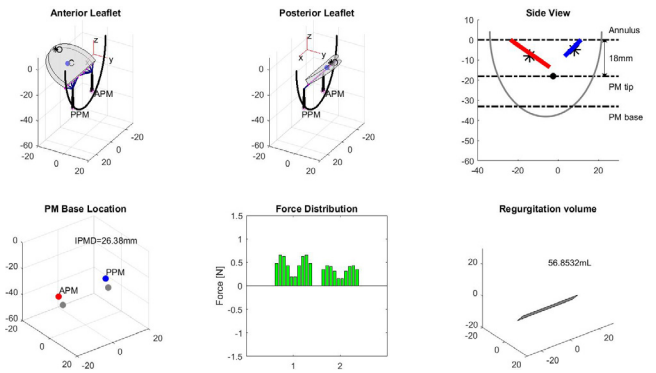

Video 10. Simulation runs for MR model II. While the normal model was built based on normal ventricular dynamics with the ventricular size of 34 mm, interpapillary muscle distance of 22 mm, and consistent annulo-PM distance, MR model was built based on MR ventricular dynamics with increased ventricular size of 42 mm, increased interpapillary muscle distance of 30 mm, and decreasing annulo-PM distance. PM position rearrangement with ΔXYZ = (5, −2.5, 5) for APM and ΔXYZ = (−5, −2.5, 5) for PPM resulted in posterior leaflet prolapse with anterior leaflet tethering creating regurgitation volume of 53.45 mL.

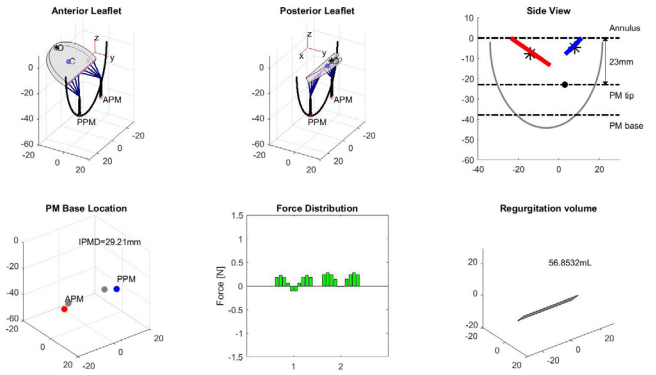

Video 11. Simulation runs for MR model III. While the normal model was built based on normal ventricular dynamics with the ventricular size of 34 mm, interpapillary muscle distance of 22 mm, and consistent annulo-PM distance, MR model was built based on MR ventricular dynamics with increased ventricular size of 42 mm, increased interpapillary muscle distance of 30 mm, and decreasing annulo-PM distance. PM position rearrangement with ΔXYZ = (1.5, 3, 0) for APM and ΔXYZ = (−1.5, 3, 0) for PPM resulted in both leaflets moving beyond annulus level, creating regurgitation volume of 64.99 mL.

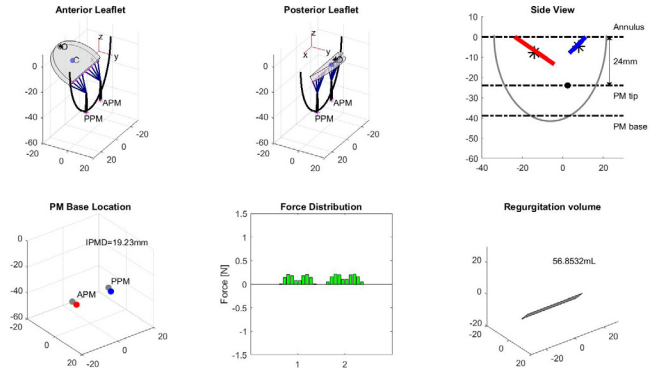

Video 12. Simulation runs for MR-fixed model. By rearranging PM positions with ΔXYZ = (6.7, 2.4, −1) and (−6.7, 2.4, −1) for APM and PPM, respectively, under the same conditions of MR model III, regurgitation volume is significantly reduced to the level of that resulted in the normal model.

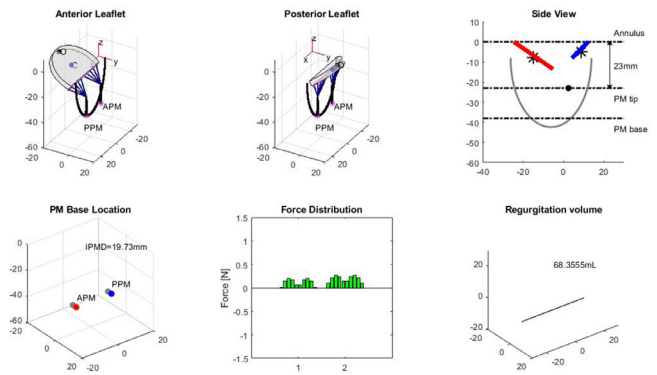

Video 13. Simulation runs for type I dysfunction. Hinge points were relocated by 2 mm farther away from each other, increasing annulus diameter from 35 mm to 37 mm. This resulted in incomplete coaptation with regurgitation volume of 58.17 mL.

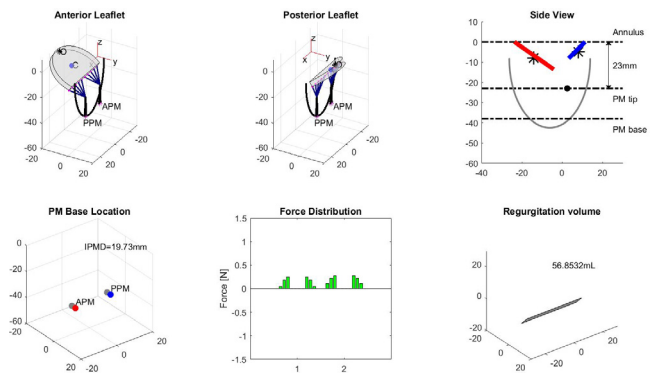

Video 14. Simulation runs for type II dysfunction with rupture of inner chordae. Elongation and rupture of chordae or PM in type II dysfunction were modeled by setting stiffness of the selected chordae tendineae as zero. Rupture of inner chordae resulted in incomplete coaptation without leaflet prolapse.

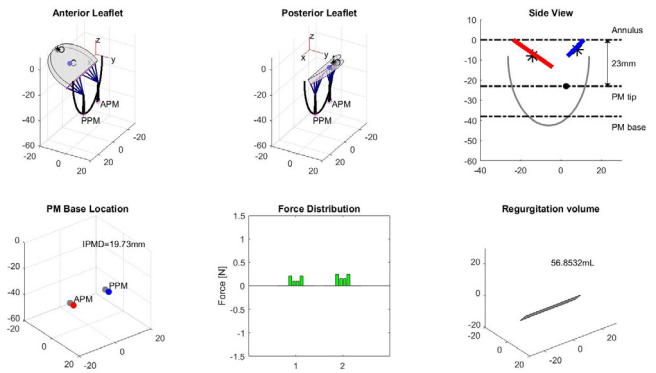

Video 15. Simulation runs for type II dysfunction with rupture of outer chordae. Elongation and rupture of chordae or PM in type II dysfunction were modeled by setting stiffness of the selected chordae tendineae as zero. Rupture of outer chordae resulted in posterior leaflet prolapse.

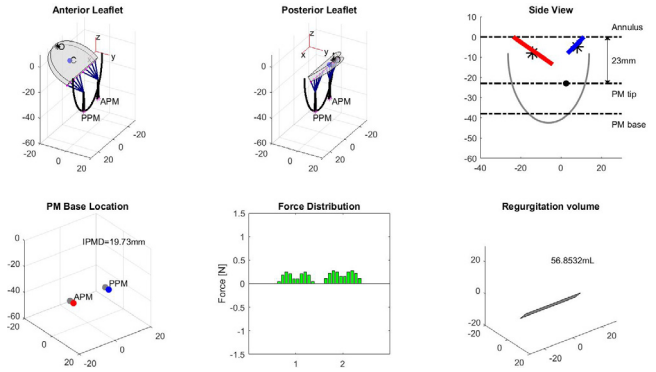

Video 16. Simulation runs for type IIIa dysfunction. Material properties of polyethylene terephthalate plastic (density = 1.541 g/cm^2) was chosen which increased the mass by approximately one and a half times for both leaflets and provided different inertia matrix. With increased mass, there was incomplete coaptation with regurgitation volume of 12.62 mL.

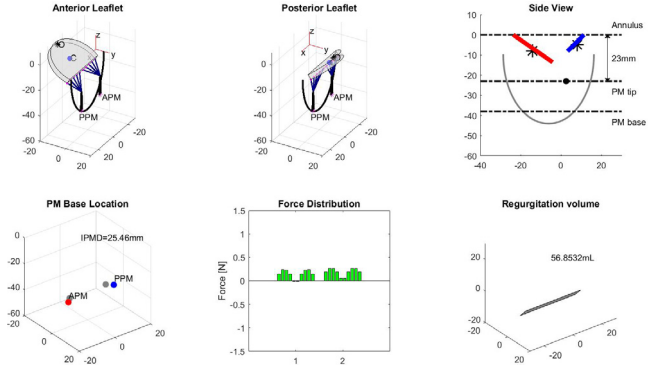

Video 17. Simulation runs for type IIIb dysfunction with PM displacement. Assuming that type IIIb dysfunction may have abnormal ventricular shape and annulo-PM dynamics similar to the MR model, we simulated type IIIb dysfunction within MR ventricular shape deformation instead of normal. As a result, there was significant movement of leaflets creating regurgitation volume of 8.293 mL.

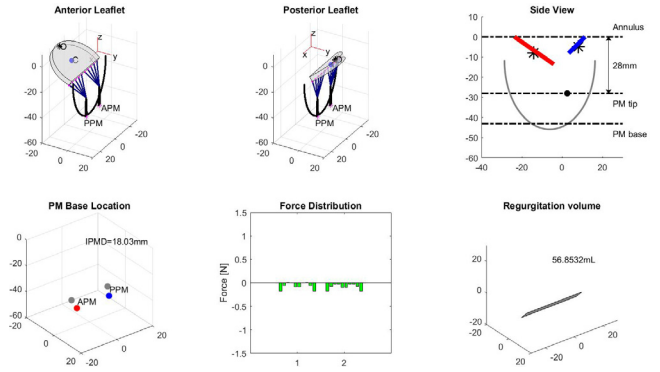

Video 18. Simulation runs for type IIIb dysfunction with chordae tethering. Assuming that type IIIb dysfunction may have abnormal ventricular shape and annulo-PM dynamics similar to the MR model, we simulated type IIIb dysfunction within MR ventricular shape deformation instead of normal. As a result, there was significant movement of leaflets creating regurgitation volume of 24.39 mL.

REFERENCES

1. Rowlatt U: Comparative anatomy of the heart of mammals. Zool J Linn Soc 98:73–110, 1990
2. Stephenson A, Adams J, Vaccarezza M: The vertebrate heart: An evolutionary perspective. J Anat 231:787–797, 2017
3. Simoes-Costa M, Vasconcelos M, Sampaio A, et al: The evolutionary origin of cardiac chambers. Dev Biol 277:1–15, 2005
4. Mick S, Keshavamurthy S, Gillinov A: Mitral valve repair versus replacement. Ann Cardiothorac Surg 4:230–237, 2015
5. Kim WK, Kim HJ, Kim JB, et al: Clinical outcomes in 1731 patients undergoing mitral valve surgery for rheumatic valve disease. Heart 104 (10):841–848, 2018.
6. Silaschi M, Chaubey S, Aldalati O, et al: Is mitral valve repair superior to mitral valve replacement in elderly patients? Comparison of short- and long-term outcomes in a propensity-matched cohort. J Am Heart Assoc 5(8):e003605, 2016.
7. Aybek T, Risteski P, Miskovic A, et al: Seven years' experience with suture annuloplasty for mitral valve repair. J Thorac Cardiovasc Surg 131:99–106, 2006
8. Acker M, Parides M, Perrault L, et al: Mitral-valve repair versus replacement for severe ischemic mitral regurgitation. N Engl J Med 370:23–32, 2014
9. Chen W, Lee T, Lee P, et al: Effects of internal stress concentrations in plantar soft-tissue—A preliminary three-dimensional finite element analysis. Med Eng Phys 32:324–331, 2010
10. Baruh H: Analytical Dynamics. Boston, MA: WCB/McGraw-Hill 1999
11. Sakai T, Okita Y, Ueda Y, et al: Distance between mitral annulus and papillary muscles: Anatomic study in normal human hearts. J Thorac Cardiovasc Surg 118:636–641, 1999
12. Lee A, Hsiung M, Salgo I, et al: Quantitative analysis of mitral valve morphology in mitral valve prolapse with real-time 3-dimensional echocardiography: Importance of annular saddle shape in the pathogenesis of mitral regurgitation. Circulation 127:832–841, 2013
13. Omran A, Arifi A, Mohamed A: Echocardiography of the mitral valve. J Saudi Heart Assoc 22:165–170, 2010
14. Nordblom P, Bech-Hanssen O: Reference values describing the normal mitral valve and the position of the papillary muscles. Echocardiography 24:665–672, 2007
15. Jimenez J, Soerensen D, He Z, et al: Mitral valve function and chordal force distribution using a flexible annulus model: An in vitro study. Ann Biomed Eng 33:557–566, 2005
16. Lang R, Badano L, Mor-Avi V, et al: Recommendations for cardiac chamber quantification by echocardiography in adults: An update from the American Society of Echocardiography and the European Association of Cardiovascular Imaging. J Am Soc Echocardiogr 28: 1−39.e14, 2015
17. Levine R, Triulzi M, Harrigan P, et al: The relationship of mitral annular shape to the diagnosis of mitral valve prolapse. Circulation 75:756–767, 1987
18. Jolley M, Ghelani S, Adar A, et al: Three-dimensional mitral valve morphology and age-related trends in children and young adults with structurally normal hearts using transthoracic echocardiography. J Am Soc Echocardiogr 30:561–571, 2017
19. Barber J, Kasper F, Ratliff N, et al: Mechanical properties of myxomatous mitral valves. J Thorac Cardiovasc Surg 122:955–962, 2001
20. McCarthy K, Ring L, Rana B: Anatomy of the mitral valve: Understanding the mitral valve complex in mitral regurgitation. Eur J Echocardiogr 11:i3–i9, 2010
21. Choi A, Zheng Y: Estimation of Young's modulus and Poisson's ratio of soft tissue from indentation using two different-sized indentors: Finite element analysis of the finite deformation effect. Med Biol Eng Comput 43:258–264, 2005
22. Votta E, Caiani E, Veronesi F, et al: Mitral valve finite-element modelling from ultrasound data: A pilot study for a new approach to understand mitral function and clinical scenarios. Philos Trans A Math Phys Eng Sci 366:3411–3434, 2008
23. Morgan A, Pantoja J, Weinsaft J, et al: Finite element modeling of mitral valve repair. J Biomech Eng 138:021009, 2016
24. Romashov Y, Kizilova N, Gaidulis G Mathematical modeling of mitral valve dynamics: Nonlinear vs linear models 2016. Proceedings of the 5th International Conference on Nonlinear Dynamics ND-KhPI2016 September 27-30, 2016, Kharkov, Ukraine
25. Kass D, Traill T, Keating M, et al: Abnormalities of dynamic ventricular shape change in patients with aortic and mitral valvular regurgitation: Assessment by Fourier shape analysis and global geometric indexes. Circ Res 62:127–138, 1988
26. Wilcox A, Buchan K, Espino D: Frequency and diameter dependent viscoelastic properties of mitral valve chordae tendineae. J Mech Behav Biomed Mater 30:186–195, 2014
27. Obadia J, Casali C, Chassignolle J, et al: Mitral subvalvular apparatus: Different functions of primary and secondary chordae. Circulation 96:3124–3128, 1997
28. Lomholt M, Nielsen S, Hansen S, et al: Differential tension between secondary and primary mitral chordae in an acute in-vivo porcine model. J Heart Valve Dis 11:337–345, 2002